JOURNAL OF AIRCRAFT
Vol. 30, No. 5, Sept.–Oct. 1993

Investigation of Vortex Development on a Pitching Slender Body of Revolution

M. J. Stanek* and M. R. Visbal*
Air Force Wright Laboratory, Wright-Patterson Air Force Base, Ohio 45433

A computational study of the unsteady flow about a pitching 3.5-caliber tangent ogive forebody is presented. The flow is simulated using the full three-dimensional unsteady Navier-Stokes equations and a time-accurate implicit algorithm. Effects of grid resolution and a comparison of solutions using full Navier-Stokes and the thin-layer approximation are included. The forebody is simulated in a "pitch-up to 20 deg and hold" maneuver, and two different pitch-axis locations are used in the study. Examination of the unsteady vorticity field for the pitch-up cases reveals the formation of strong shear layers as the body decelerates, and their roll-up into vortical structures in a process similar to that observed in airfoil dynamic stall. Pronounced vortex/surface interactions are seen which produce multiple secondary separation regions, ejection of vorticity from the surface, and embedded regions of high suction.

Nomenclature

C_{nf}	=	sectional normal force coefficient, $F_n/q_\infty D$
C_p	=	pressure coefficient, $2(p - p_\infty)/\rho_\infty U_\infty^2$
D	=	body diameter
F_n	=	normal force per unit length
L	=	length from ogive tip to pitch axis
L_0	=	length of ogive section
$\hat{n}$	=	body normal unit vector
p	=	pressure
q_∞	=	dynamic pressure, $\frac{1}{2}\rho_\infty U_\infty^2$
Re_D	=	Reynolds number, $\rho_\infty U_\infty D/\mu_\infty$
T	=	temperature
t	=	time
U	=	velocity
x, y, z	=	Cartesian coordinates
x_τ, y_τ, z_τ	=	velocity components of moving grid
α	=	angle of attack, deg
ξ, η, ζ	=	transformed coordinates
ρ	=	density
τ	=	nondimensional time, tU_∞/L_0
Ω^+	=	nondimensional pitch rate, $\omega L_0/U_\infty$
ω	=	pitch rate, rad/s
ω'	=	nondimensional pitch rate, $\omega L/U_\infty$
ω_x	=	streamwise component of vorticity

Subscripts

b	=	value on body surface
max	=	maximum value
∞	=	freestream value

Introduction

THE desire to enhance the maneuverability of future fighter aircraft and missiles has resulted in an increased emphasis on the unsteady vortical flows produced by moving aerodynamic surfaces.[1] One phenomenon which prevents designers from making full use of vortical flows (particularly those on the lee side of slender forebodies) in modern missile and aircraft designs, is the readiness of leeward vortices to develop asymmetrically. Although it is quite important to study vortex asymmetries at fixed high incidence,[2–10] it is also important to start to examine the effect of maneuvering into a fixed angle of attack. Techniques developed for controlling vortex asymmetry on slender forebodies may eventually have to take into account the motion of the body as well as flowfield history effects. Ericsson,[11] for example, has suggested that the "moving-wall" effect will completely overpower the effect of asymmetry on slender forebodies for certain types of maneuvers. These facts serve to illustrate the need for detailed experimental and computational investigations of maneuvering slender forebodies.

Experimental data for pitching ogives/cones is sparse, and limited to integrated force and moment results or to flow visualizations. Smith and Nunn[12] studied a three-caliber ogive forebody pitching at constant rate about its midpoint. They presented comparisons of normal force, pitching moment, and center of pressure (c.p.) data for both static and dynamic cases. The relatively low pitch rates ($\omega' < 0.036$) considered resulted mainly in slight angular delays in the leeside vortex development.

Gad-el-Hak and Ho[13] investigated a three-caliber ogive forebody pitching harmonically about its midpoint from 0 to 30 deg. Moderate to high oscillation rates ($0.1 \leq \omega'_{\max} \leq 2.0$) were considered, and the growth/decay cycle of the vortical structures was described.

The most recent pitching forebody experimental study was conducted by Montividas et al.[14] The purpose of that study was to map the various flow regimes of a pitching cone forebody for various Reynolds numbers, pitch rates ($-0.35 < \omega' < 0.35$), and pitch axis locations. Montividas also showed that for pitching forebodies a suitable nondimensional pitch rate for comparing sets of data is defined as $\omega' = \omega L/U_\infty$, where ω is the angular rate, U_∞ is the freestream velocity, and L is the distance from the tip of the body to the pitch axis. This nondimensional pitch-rate definition is adopted in this article.

No experimental results exist which shed light on details of vortex formation and subsequent unsteady development. In addition, none of the pitching forebody experiments offer any quantitative unsteady flow data (such as velocity or pressures) which could be used for validation purposes. To the authors knowledge, the only Navier-Stokes computation of a pitching forebody ($\omega' \simeq 0.2$) was performed by Ying et al.[15] This work simulated a hemisphere cylinder in pitch-up to 19 deg at a freestream Mach number of 1.2. Time histories of pressures on the body and various force coefficients were presented, but no details of the unsteady evolution of the flow structure were given.

Presented as Paper 91-3273 at the AIAA 9th Applied Aerodynamics Conference, Baltimore, MD, Sept. 23–25, 1991; received Sept. 26, 1991; revision received June 8, 1992; accepted for publication June 10, 1992.

*Aerospace Engineer, Flight Dynamics Directorate. Member AIAA.

The main objective of this work is to describe in detail the complex unsteady three-dimensional vortex development surrounding an ogive forebody in a pitch-up and hold maneuver. A previously developed and validated three-dimensional time-accurate Navier-Stokes code has been utilized to compute both steady angle of attack (for validation) and pitching forebody cases. This pitching ogive simulation is seen as an initial step toward future maneuvering fighter aircraft and missile simulations.

The effects of pitching motion on vortex development were examined by looking at a 3.5-caliber tangent ogive forebody in a pitch-up and hold maneuver (0–20 deg). Two pitch-axis locations were used giving values for ω' of 0.5 and 1.5. Included in this work is a limited grid resolution study and a comparison between solutions using full Navier-Stokes equations and the thin-layer approximation. A steady validation case including grid resolution effects is given in Ref. 16.

Governing Equations and Numerical Procedure

The governing equations utilized in this study are the full unsteady, three-dimensional compressible Navier-Stokes equations written in strong conservative form.[17] Closure of this system of equations is provided by the perfect gas law, Sutherland's viscosity formula, and the assumption of a constant molecular Prandtl number.

For the case of external flow past a body in arbitrary motion, the governing equations can be formulated using two different approaches. In the first approach, the flow equations are written in a noninertial frame of reference attached to the body. While this avoids the use of a moving grid, it requires the introduction of ficticious acceleration terms into the governing equations. In the second approach, selected for this study, the velocity is defined in the inertial system, and motion of the body is provided for by means of a general time-dependent coordinate transformation [$\xi = \xi(x, y, z, t)$, $\eta = \eta(x, y, z, t)$, $\zeta = \zeta(x, y, z, t)$, $\tau = t$].

The governing equations are solved using the implicit, approximate-factorization algorithm of Beam and Warming.[18] The scheme is formulated using Euler implicit time-differencing and second-order finite difference approximations for all spatial derivatives. A combination of second- and fourth-order dissipation[19] is added to maintain the numerical stability of the central difference scheme. Only fourth-order dissipation was required for the current subsonic flow investigation. A Newton subiteration procedure[20] is incorporated in the numerical scheme to reduce factorization/linearization errors and to enhance the stability characteristics of the solver. Metric averaging has also been employed to insure that the geometric conservation law is satisfied.[17]

A Navier-Stokes code implementing this scheme has been previously developed[21] and successfully validated for a variety of both steady and unsteady laminar test flow cases, including flow about a supersonic delta wing,[22] Taylor vortex flow,[21] unsteady subsonic delta wing flow,[23] and unsteady laminar juncture flow.[24] The unsteady laminar juncture flow and subsonic delta wing studies are of particular importance in that they demonstrate the ability of the code to correctly simulate naturally occurring instabilities in the flowfield and the transition of these flows from steady to unsteady behavior.

Grid Structure and Boundary Conditions

The grid developed for this study is of the C-O type (see Fig. 1). A nearly orthogonal, two-dimensional boundary-fitted mesh is generated about the ogive-cylinder employing a hyperbolic grid-generation procedure.[25,26] This C-grid is then rotated about the longitudinal axis of the body to construct the three-dimensional grid. On all grids used in this study, the spacing normal to the body at the wall was set equal to $0.0001L_0$. The minimum grid cell spacing in the ξ direction was set to $0.0013L_0$. The tip of the body was rounded with a radius of curvature of $0.026L_0$. The far-field boundary was fixed at a minimum of 22-diam away from the body surface.

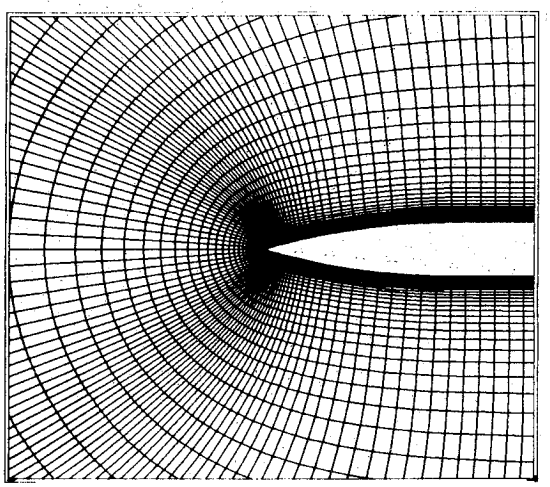

Fig. 1 C-O grid structure.

The time-dependent coordinate transformation is implemented using a rigid, nondeforming grid attached to the forebody. Once the grid at zero angle of attack is constructed, the physical coordinates (x, y, z) and grid velocity (x_τ, y_τ, z_τ) are easily computed as a function of the body angle-of-attack $\alpha(t)$ and the prescribed angular velocity $\omega(t)$.

The boundary conditions are prescribed as follows. Along the far-field boundary, freestream conditions are given. First-order extrapolation is used on the outflow boundary for all variables. On the forebody surface, the following condition is applied:

$$\boldsymbol{U} = \boldsymbol{U}_b \tag{1}$$

$$\frac{\partial T}{\partial \eta} = 0 \tag{2}$$

$$\frac{\partial p}{\partial n} = -\rho \boldsymbol{a}_b \cdot \hat{\boldsymbol{n}} \tag{3}$$

where $\boldsymbol{U}_b$ and $\boldsymbol{a}_b$ denote, respectively, the velocity and acceleration on the ogive surface given by the prescribed pitching motion.[16]

A line of singularity in the coordinate transformation lies along the longitudinal axis and extends from the tip of the ogive to the upstream far-field boundary. The flow variables along this line were simply set equal to the average of the flow variables on the adjacent ξ surface. For some of the pitching cases, the flow is assumed to have bilateral symmetry with respect to the x-y plane; therefore, $w = 0$, and $\partial/\partial\zeta = 0$ for all the remaining variables. For cases where no symmetry was assumed, a five-plane overlap in the ζ direction was used on the windward side of the body.

Results and Discussion

Two primary unsteady pitch-up and hold cases are considered. The freestream Mach number and Reynolds number (Re_D) are 0.28 and 2×10^4, respectively. In both cases, the forebody is pitched at the same angular rate; what differs is the location of the pitch axis. This yields two values ω' of 0.5 and 1.5. Two grids are used for the unsteady cases with the following dimensions in the axial, body normal, and azimuthal directions: $72 \times 63 \times 61$ (coarse, half-grid with assumed symmetry) and $110 \times 63 \times 125$ (fine, full grid). All unsteady cases were run at a nondimensional time step $\Delta\tau = 0.001$ using three subiterations. It should be noted that even without subiterations the scheme is temporally accurate, and subiterations are mainly employed to enhance numerical stability.

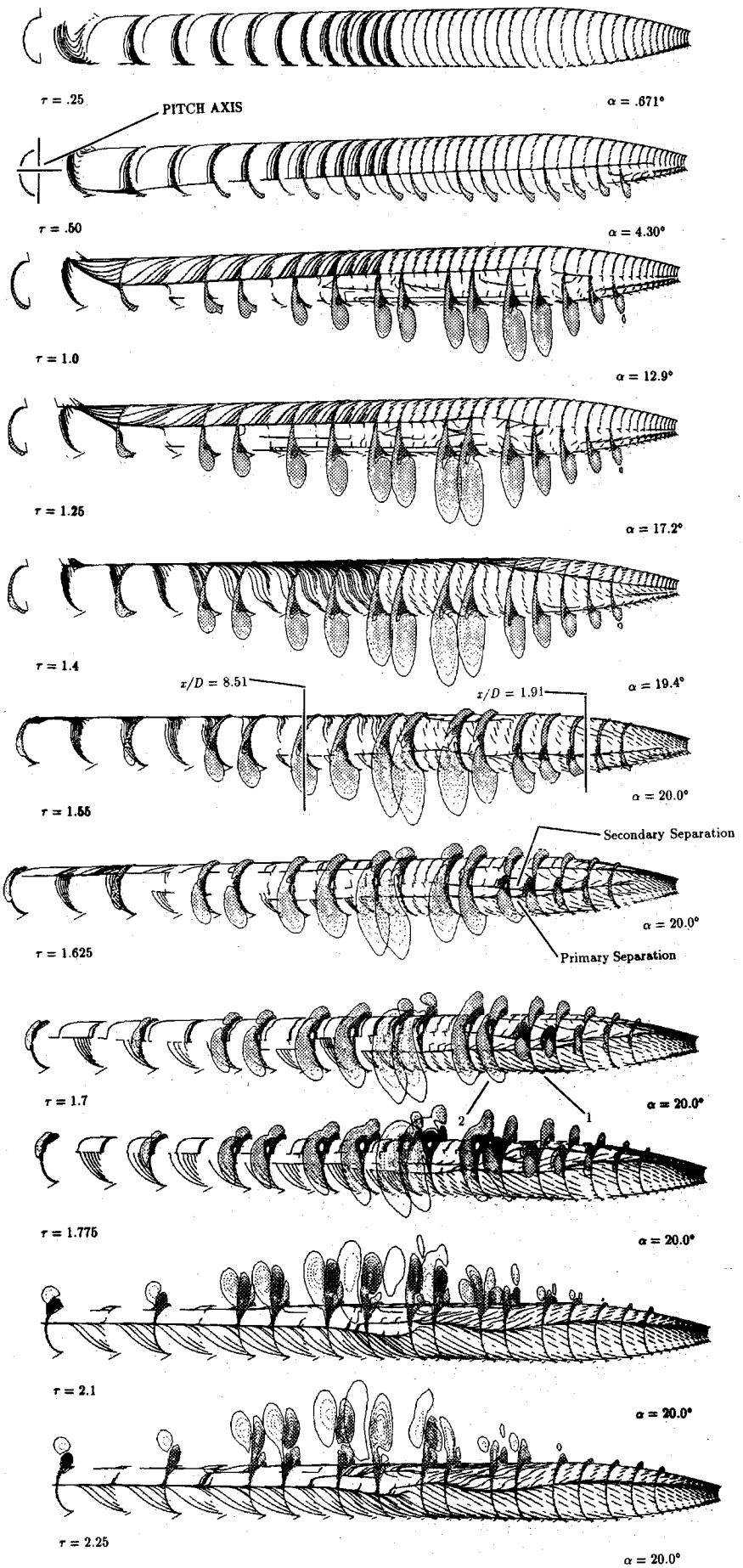

Fig. 2 Time sequence showing the evolution of streamwise component of vorticity contours and instantaneous surface shear pattern on pitching forebody for $\omega' = 1.5$.

Starting with a converged solution at $\alpha = 0$ deg, the forebody was smoothly accelerated to a constant pitch rate, pitched at a constant rate, smoothly decelerated to a zero pitch rate, and then held fixed at $\alpha = 20$ deg. Due to space limitations, only results for $\omega' = 1.5$ are presented below. Results for the case of $\omega' = 0.5$ can be found in Ref. 16.

$\omega' = 1.5$

In the first pitch-up case, the pivot point was located 17 diam from the nose tip on the longitudinal axis of the forebody, at the last axial grid station. Figure 2 shows a time sequence of axial component of vorticity contours superimposed on the surface flow pattern.

The limiting streamline patterns are computed in the frame of reference moving with the body. Figures 3 and 4 show more clearly the evolution of the vorticity field at two axial stations, $x/D = 1.91$ and $x/D = 8.51$.

For $\tau < 0.25$, the surface flow pattern on the moving body shows a strong downward crossflow in response to the upward pitch. For this case, with the pitch axis located at the rear of the computational grid, all of the crossflow velocity induced by the pitching motion is, as expected, directed downward. For $\tau < 0.25$, the vorticity is bound in a thin layer close to the body surface. By $\tau = 0.5$, the body has accelerated to a constant pitch rate. A primary separation line appears over the entire length of the forebody, and signals the roll-up of the thin layer of vorticity into a primary vortical structure. The sense of rotation of this structure is negative or counterclockwise when viewed from the ogive tip.

From $\tau = 1.0$ to 1.25 (see Fig. 3), one observes the growth of the primary (counterclockwise) vortex as well as the de-

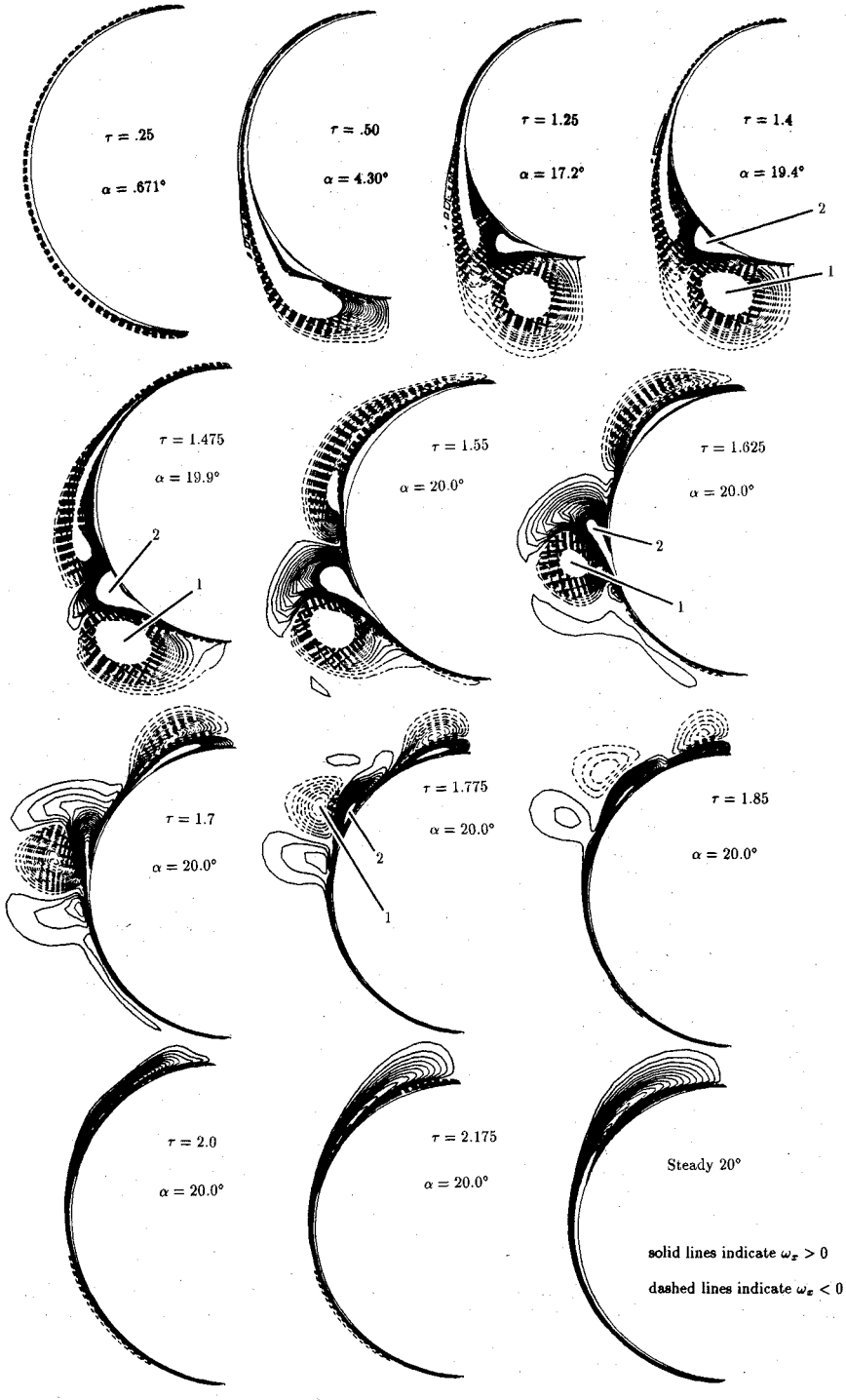

Fig. 3 Evolution of streamwise vorticity contours at an axial section ($x/D = 1.91$) on the ogive forebody (see Fig. 2 for relative axial position).

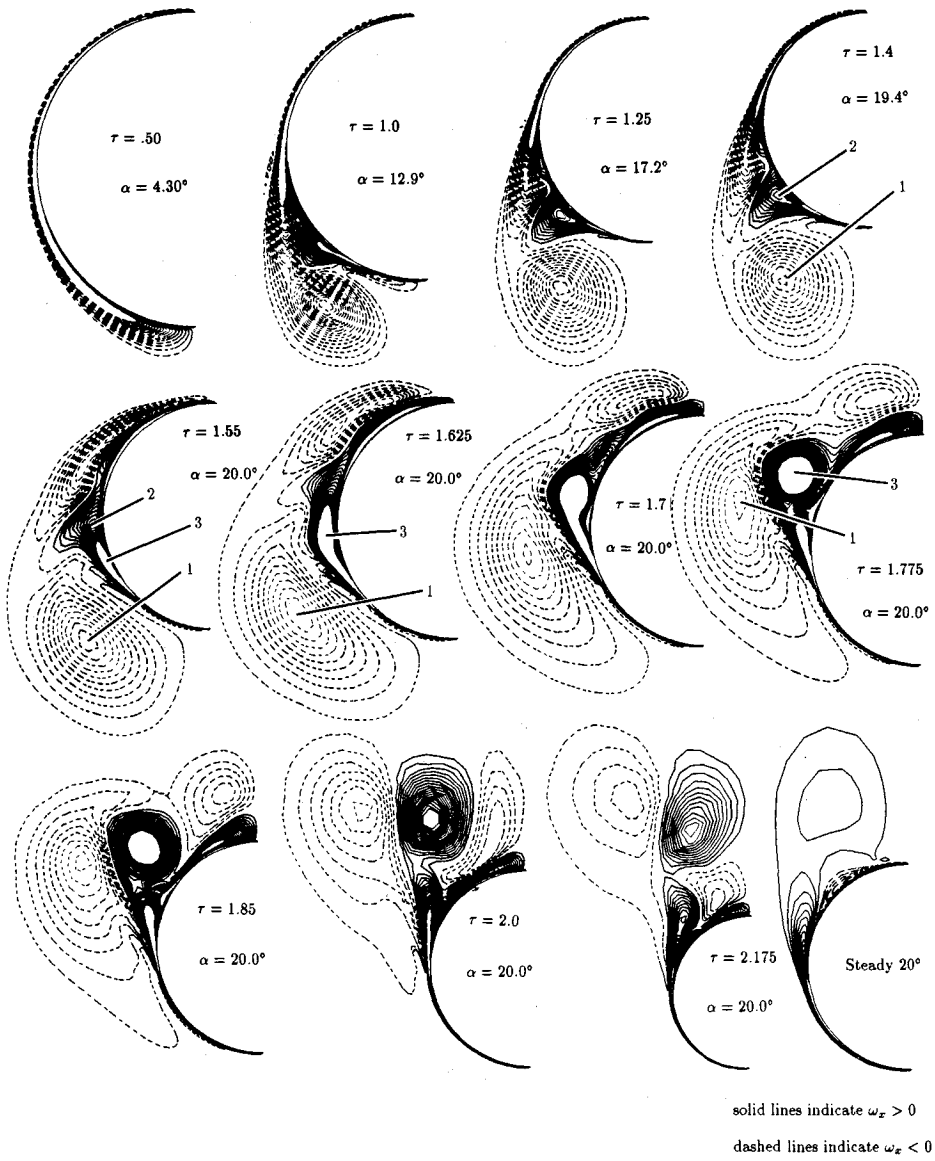

Fig. 4 Evolution of streamwise vorticity contours at an axial section (x/D = 8.51) on the ogive forebody (see Fig. 2 for relative axial position).

velopment of a secondary (clockwise) structure. At τ = 1.25 (Fig. 2), the vortical structure on the underside of the forebody is seen to grow from the ogive tip to a maximum near the ogive shoulder, and then decreases in size as the pivot axis is approached. For this pitching case a relative crossflow component is provided by the motion, and varies linearly with x from a maximum ($L\omega$) at the tip to zero at the pitch axis. To a first approximation, the body motion results in an effective local angle of attack which changes along the longitudinal axis. At the time the forebody achieves a constant pitch rate, the induced negative angle of attack varies from approximately −56 deg at the nose tip to zero at the pivot point. The complex and interrelated effects of local effective angle of attack, cross-sectional area variation, and vorticity convection results in the downstream growth and subsequent decay of the motion-induced vortical structure observed on the underside of the body.

From τ = 1.25 to 1.55, the forebody undergoes a strong angular deceleration. At τ = 1.4, the surface flow pattern (Fig. 2) shows that the predominant crossflow direction has changed from downward to upward, yet little change is apparent in the main vortical structure. This indicates that a very strong thin shear layer of positive vorticity is developing on the surface of the body. The primary separation line which at τ = 1.25 spans the entire length of the body, by τ = 1.4 only persists at the front of the ogive. From this point onward, the main crossflow is directed upward, and the separation lines on the body surface are associated with the newly formed thin clockwise shear layer. By τ = 1.55, the forebody has stopped at α = 20 deg, and one can observe (Fig. 2) a new primary separation line. It should be noted that now, with the crossflow directed upward, the new developing primary vortical structures contain clockwise vorticity.

In Figs. 2 and 4, at τ = 1.625 and τ = 1.7, the roll-up of the new shear layer of clockwise vorticity is apparent. This can also be observed in the close-up in Fig. 5. In addition, Fig. 5 shows that different behavior in the evolution of the vorticity exists at different axial positions along the forebody (compare stations 1 and 2 in Figs. 2 and 5).

Examination of the flow evolution at x/D = 1.91 (Fig. 3) shows that as the body decelerates and comes to a stop (τ = 1.25–1.55), the previous secondary clockwise structure (denoted as "2") becomes stronger. As the clockwise structure 2 gains strength, it succeeds in tearing the counterclockwise vortex "1" from its feeding sheet (τ = 1.475, Fig. 3). Even though the vortex 1 is separated from its feeding shear layer, it is still strong enough (possibly subject to intensification by stretching) and sufficiently close to the wall to induce an "eruption" of positive vorticity. In the sequence τ = 1.55–1.7, the vortical structure 2 actually wraps around and engulfs the primary vortex 1. This is analogous to phenomena observed in unsteady laminar juncture flows.[24,27,28] With the

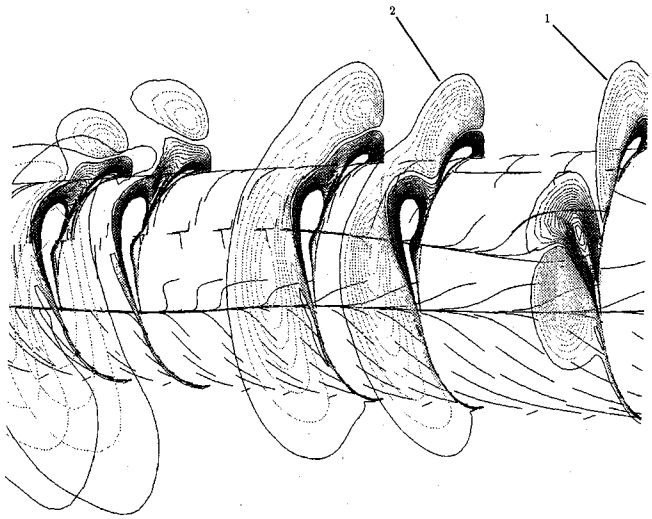

Fig. 5 Close-up of vorticity contours and flow lines at $\tau = 1.7$ showing shear layer roll-up (dynamic stall-like structure) and rapid change in structure from station 1 to 2.

dominant crossflow now upward, structures 1 and 2 are seen to convect in a clockwise fashion around the body.

In Fig. 4, at $x/D = 8.51$, a somewhat different evolution of the vortical structures is observed. From $\tau = 1.4$ to 1.25, the old secondary vortex 2 is convected clockwise and eventually loses its identity as it merges with the new wall shear layer. From $\tau = 1.55$ to 1.775, the intense shear layer "3" rolls up into a strong, well-defined vortex. This dramatic shear layer roll-up is somewhat similar to the dynamic-stall vortex formation on a pitching airfoil.[29,30] As in dynamic stall, the energetic vortical structure 3 results in a thin band of high suction along the midsection of the body, with local surface pressure coefficients as low as -6.25.

As Figs. 2–4 indicate, the original old primary vortex structures which have been split by the developing new primary vortex, continually weaken as they are convected downstream and around the body in a clockwise direction. At section $x/D = 8.51$ in Fig. 4, the dynamic stall-like vortex grows in size as it evolves into the new primary vortex.

In Fig. 3, by $\tau = 2.175$ at the upstream station $x/D = 1.91$, the vorticity field has relaxed back to a condition which is quite close to the steady state. However, at the downstream station $x/D = 8.51$, by the same time (Fig. 4), the flow is clearly far from its final steady condition. At the time when the computation was stopped ($\tau = 2.25$), the new primary line of separation in Fig. 2 still exhibits unsteady behavior downstream of the ogive shoulder. However, on the ogive section, the primary line looks quite similar to the steady case.[16] It should be noted that no secondary separation line is visible yet. Although finding the time required for the entire flowfield to relax to a steady state is of interest, this was not possible due to limitations in computer resources.

Figures 6 and 7 show, respectively, the history of the normal force coefficient at $x/L_0 = 1.7$, as well as the history of the total normal force coefficient. It is evident that the total lift of the forebody correlates well with this sectional normal force. Notice also in both figures, the lift overshoot present at $\tau = 1.75$ which occurs after the forebody has already come to rest. Finally, by $\tau = 2.25$, the lift in both plots is very close to the respective steady-state values.

Effects of Grid Resolution, Secondary Viscous Terms, and Symmetry Conditions

The pitch-up case with $\omega' = 1.5$ was simulated on a $72 \times 63 \times 61$ grid, assuming symmetry by solving the thin-layer Navier-Stokes equations. In the thin-layer approximation, only

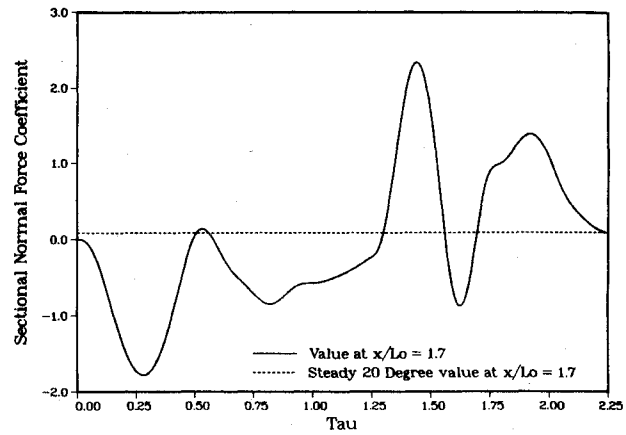

Fig. 6 Time history of sectional normal force coefficient at $x/L_0 = 1.7$ for $\omega' = 1.5$. Body motion has ceased by $\tau = 1.55$.

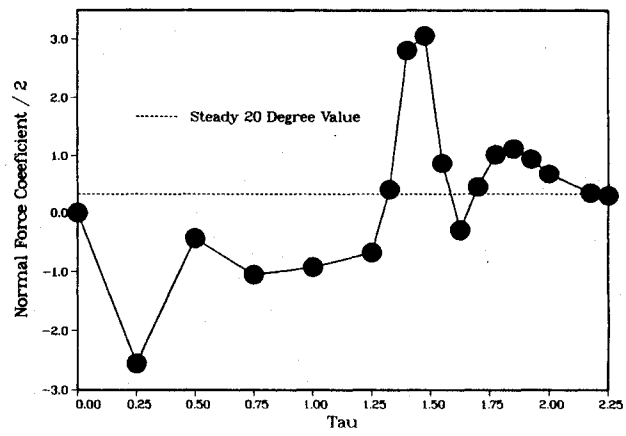

Fig. 7 History of body normal force coefficient at selected times for $\omega' = 1.5$. Body motion has ceased by $\tau = 1.55$.

viscous terms normal to the body are computed. This assumption is widely used in the simulation of high Reynolds number flows. Two additional calculations were performed for $\omega' = 1.5$ to investigate the suitability of the thin-layer assumption, the effect of grid resolution and the possible appearance of flow asymmetries. The second calculation was performed on the same half-grid ($72 \times 63 \times 61$) using the full Navier-Stokes equations to isolate the effect of the secondary viscous terms neglected in the thin-layer approximation. A third calculation was performed on a finer whole grid ($110 \times 63 \times 125$, no assumed symmetry) where the axial resolution was effectively doubled in the primary region of interest ($x/D = 3.5$ to $x/D = 14$) to investigate the effect of grid resolution, as well as to allow for the appearance of unforeseen flow asymmetries. Figure 8 shows a comparison of these three calculations at $\tau = 1.85$. No appreciable difference exists between the thin-layer and Navier-Stokes solutions, even for this extremely complex unsteady flow. Slight differences exist between the coarse and fine grid solutions, but they are limited to small variations in the surface shear patterns. However, the computed evolution in time of the main vortical structures are the same for both grids.

The fine, whole grid solution did not exhibit any hint of asymmetric behavior. This conclusion was based upon visual inspection of crossflow vorticity contours and constant monitoring of the sectional side force coefficient at several axial stations. This result was not unexpected, since the steady $\alpha = 20$-deg case was shown experimentally[2] to be symmetric. In addition, pitching experiments by Montividas et al.[14] showed that pitching-up produces a lag in the appearance of vortex asymmetry.

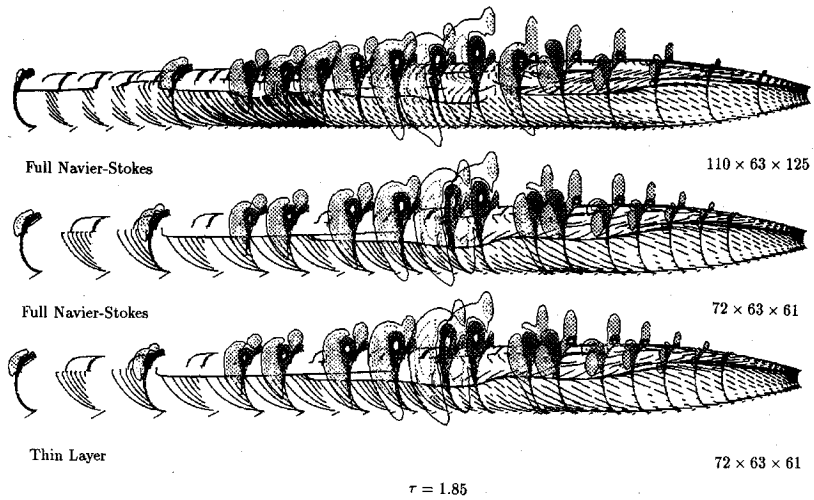

Fig. 8 Comparison of vortical structure and surface pattern among fine grid/full Navier-Stokes, coarse grid/full Navier-Stokes, and coarse grid/thin-layer results ($\omega' = 1.5$).

Concluding Remarks

A validated, time-accurate Navier-Stokes solver has been used to study the transient development of the vortical structures surrounding an axisymmetric forebody in a pitching maneuver. For the pitch-up case with $\omega' = 1.5$, the intense deceleration of the body results in the formation of a strong shear layer which rolls up into a vortical structure in a process that is similar to that observed in airfoil dynamic stall. In addition, a pronounced vortex/surface interaction results in the ejection of vorticity from the surface. The roll-up of a dynamic stall-like vortex induces localized regions of high suction on the body surface, as well as a strong lift overshoot. Local sectional normal force coefficients seven times as high as the maximum value for the steady 20-deg case are observed. A comparison of results obtained on two different grids showed that the overall development of the main vortical structures was the same. In addition, comparison of computed results using the thin-layer and full Navier-Stokes equations showed no appreciable difference. Finally, at no time during the whole grid calculation did the solution exhibit any sign of vortex asymmetry.

In closing, it should be noted that detailed unsteady experimental measurements are required to provide additional insight into these complex maneuvering body flowfields, and this data is sorely needed to provide the necessary validation for current and future numerical flow solvers.

Acknowledgment

Computational resources for the present study were provided by NASA Ames Research Center, under the Numerical Aerodynamic Simulation Program.

References

[1]Lang, J. D., and Frances, M. S., "Unsteady Aerodynamics and Dynamic Aircraft Maneuverability," AGARD Symposium on Unsteady Aerodynamics—Fundamentals and Applications to Aircraft Dynamics, Gottingen, Germany, May 1985.

[2]Lamont, P. J., "The Complex Asymmetric Flow over a 3.5D Ogive Nose and Cylindrical Afterbody at High Angle of Attack," AIAA Paper 82-0053, Jan. 1982.

[3]Degani, D., and Schiff, L. B., "Numerical Simulation of the Effect of Spatial Disturbances on Vortex Asymmetry," AIAA Paper 89-0340, Jan. 1989.

[4]Kandil, O. A., Wong, T. C., and Liu, C. H., "Navier-Stokes Computations of Symmetric and Asymmetric Vortex Shedding Around Slender Bodies," AIAA Atmospheric Flight Mechanics Conf., AIAA Paper 89-3397-CP, Aug. 1989.

[5]Degani, D., "Numerical Investigation of the Origin of Vortex Asymmetry," AIAA Paper 90-0593, Jan. 1990.

[6]Zilliac, G., Degani, D., and Tobak, M., "Asymmetric Vortices on a Slender Body of Revolution," AIAA Paper 90-0388, Jan. 1990.

[7]Hartwich, P. M., and Hall, R. M., "Navier-Stokes Solutions for Vortical Flows over a Tangent-Ogive Cylinder," *AIAA Journal*, Vol. 28, No. 7, 1990, pp. 1171–1179.

[8]Degani, D., and Tobak, M., "Numerical, Experimental, and Theoretical Study of Convective Instability of Flows over Pointed Bodies at Incidence," AIAA Paper 91-0291, Jan. 1991.

[9]Schiff, L. B., Degani, D., and Gavali, S., "Numerical Simulation of Vortex Unsteadiness on Slender Bodies of Revolution at Large Incidence," AIAA Paper 89-0195, Jan. 1989.

[10]Degani, D., and Zilliac, G. G., "Experimental Study of Unsteadiness of the Flow Around an Ogive-Cylinder at Incidence," AIAA Atmospheric Flight Mechanics Conf., AIAA Paper 88-4330-CP, 1988.

[11]Ericsson, L. E., "The Fickle Effect of Nose Microasymmetry on the High Alpha Aerodynamics," AIAA Paper 90-0067, Jan. 1990.

[12]Smith, L. H., and Nunn, R. H., "Aerodynamic Characteristics of an Axisymmetric Body Undergoing a Uniform Pitching Motion," AIAA Paper 75-0638, June 1975.

[13]Gad-el Hak, M., and Ho, C., "Unsteady Flow Around an Ogive Cylinder," *Journal of Aircraft*, Vol. 23, No. 6, 1986, pp. 520–528.

[14]Montividas, R. E., Reisenthel, P., and Nagib, H. N., "The Scaling and Control of Vortex Geometry Behind Pitching Cylinders," AIAA Paper 89-1003, March 1989.

[15]Ying, S. X., Steger, J. L., Schiff, L. B., and Baganoff, D., "Numerical Simulation of Unsteady, Viscous, High-Angle-of-Attack Flows Using a Partially Flux-Split Algorithm," AIAA Paper 86-2179, Aug. 1986.

[16]Stanek, M. J., and Visbal, M. R., "Investigation of Vortex Development on a Pitching Slender Body of Revolution," AIAA Paper 91-3273, Sept. 1991.

[17]Pulliam, T. H., and Steger, J. L., "On Implicit Finite-Difference Simulations of Three-Dimensional Flow," AIAA Paper 78-10, Jan. 1978.

[18]Beam, R. M., and Warming, R. F., "An Implicit Factored Scheme for the Compressible Navier-Stokes Equations," *AIAA Journal*, Vol. 16, No. 4, 1978, pp. 393–402.

[19]Jameson, A., and Baker, T., "Solution of the Euler Equations for Complex Configurations," AIAA Paper 83-1929, July 1983.

[20]Gordnier, R. E., and Visbal, M. R., "Unsteady Navier-Stokes Solutions for a Low Aspect Ratio Delta Wing," AIAA Paper 90-1538, Jan. 1990.

[21]Visbal, M., "Numerical Investigation of Laminar Juncture Flows," AIAA Paper 89-1873, June 1989.

[22]Webster, W., and Shang, J., "Thin Layer and Full Navier-Stokes Simulations over a Supersonic Delta Wing," *AIAA Journal*, Vol. 29, No. 9, 1991, pp. 1363–1369.

[23]Gordnier, R. E., and Visbal, M. R., "Numerical Simulation of the Unsteady Vortex Structure over a Delta Wing," AIAA Paper 91-1811, June 1991.

[24]Visbal, M. R., "Structure of Laminar Juncture Flows," *AIAA Journal*, Vol. 29, No. 8, 1991, pp. 1273–1282.

[25]Steger, J., and Chaussee, D., "Generation of Body-Fitted Co-

ordinates Using Hyperbolic Partial Differential Equations," *Journal of Scientific and Statistical Computing*, Vol. 1, Dec. 1980, pp. 431–437.

[26]Kinsey, D. W., and Barth, T. J., "Description of a Hyperbolic Grid Generator Procedure for Arbitrary Two-Dimensional Grids," Air Force Wright Aeronautical Laboratories TM-84-191-FIMM, July 1984.

[27]Visbal, M. R., "The Laminar Horseshoe Vortex System Formed at a Cylinder/Plate Juncture," AIAA Paper 91-1826, June 1991.

[28]Greco, J., "The Flow Structure in the Vicinity of a Cylinder-Flat Plate Junction: Flow Regimes, Periodicity, and Vortex Interactions," M.S. Thesis, Dept. of Mechanical Engineering and Mechanics, Lehigh Univ., Bethlehem, PA, 1990.

[29]Visbal, M. R., "Dynamic Stall of a Constant-Rate Pitching Airfoil," *Journal of Aircraft*, Vol. 27, No. 8, 1990, pp. 400–407.

[30]Visbal, M. R., and Shang, J. S., "Investigation of the Flow Structure Around a Rapidly Pitching Airfoil," *AIAA Journal*, Vol. 27, No. 8, 1989, pp. 1044–1051.